Research Square

Preprints are preliminary reports that have not undergone peer review.
They should not be considered conclusive, used to inform clinical practice,
or referenced by the media as validated information.

PAX9 regulates periodontal ligament stem cell-like differentiation of human induced pluripotent stem cells

Risa Sugiura
Kyushu University
Sayuri Hamano
Kyushu University
Atsushi Tomokiyo (tomokiyo@dent.kyushu-u.ac.jp)
Kyushu University
Daigaku Hasegawa
Kyushu University
Shinichiro Yoshida
Kyushu University
Hideki Sugii
Kyushu University
Shoko Fujino
Kyushu University
Orie Adachi
Kyushu University
Masataka Kadowaki
Kyushu University
Daiki Yamashita
Kyushu University
Hidefumi Maeda
Kyushu University

Article

Keywords: induced pluripotent stem cells, periodontal ligament stem cells, extracellular matrix, transcription factor, PAX9

Posted Date: July 27th, 2022

DOI: https://doi.org/10.21203/rs.3.rs-1826621/v1

License: This work is licensed under a Creative Commons Attribution 4.0 International License. Read Full License

Abstract

Periodontal ligament stem cells (PDLSCs) play central roles in periodontal ligament (PDL) tissue homeostasis, repair, and regeneration. Previously, we established a protocol to differentiate human induced pluripotent stem cell-derived neural crest-like cells (iNCs) into PDLSC-like cells (iPDLSCs) using human PDL cell-derived extracellular matrix (ECM). However it remained unclear what factors principally regulate the differentiation of iNCs into iPDLSCs. In this study, we aimed to identify the transcription factor regulating production of human PDL cell-derived ECM, which is responsible for the generation of iPDLSCs. We cultured iNCs on two human PDL cell lines (HPDLC-3S and HPDLC-3U) and human dermal fibroblasts (HDF). iNCs cultured on HPDLC-3U showed higher iPDLSC-associated gene expression and mesenchymal differentiation capacity than cells cultured on HDF or HPDLC-3S. The transcription factor *PAX9* was highly expressed in HPDLC-3U compared with HDF and HPDLC-3S. iNCs cultured on siPAX9-transfected HPDLC-3U displayed downregulation of iPDLSC-associated marker expression and adipocytic differentiation capacity relative to controls. Our findings suggest that PAX9 is one of the transcription factors regulating ECM production in human PDL cells, which is responsible for the differentiation of iNCs into iPDLSCs.

Introduction

Periodontal ligament (PDL) is a highly specialized fibrous connective tissue that plays important roles in anchoring the tooth to the socket bone and regulating proper tooth homeostasis, repair, and nutrition [1]. One of the main causes of PDL destruction is an advanced inflammatory disease of tissues surrounding the tooth structure, periodontitis. Once PDL is lost by the progression of periodontitis, the socket bone becomes detached from the tooth root and can no longer provide support for the tooth. PDL destruction can ultimately result in tooth loss; therefore, researchers have tried to repair and regenerate injured PDL tissue with the aim of preserving teeth with severe periodontitis.

PDL consists of a heterogeneous cell population, including fibroblasts, osteoblasts, cementoblasts, endothelial cells, and epithelial cell rests of Malassez [2]. Additionally, PDL contains a subpopulation of mesenchymal stem cells. Seo et al. isolated somatic mesenchymal stem cells from PDL tissues (periodontal ligament stem cells, PDLSCs) of surgically extracted human third molars, which showed multipotency, high proliferative capacity, and the ability to regenerate bone, cementum, and PDL tissue [3]. PDLSCs also exhibit immunomodulatory abilities via suppression of T cell, B cell, and dendritic cell activities, and promotion of Treg generation [4] [5] [6] [7]. In addition, autologous human PDLSC transplantation can reduce the clinical attachment level, probing depth, and defect area, and increase bone density [8]. Therefore, PDLSCs are considered to be crucial for the repair and regeneration of PDL tissue. However, the stem cell population in PDL tissue is extremely rare, as with many other tissues, and tooth extraction is required to obtain PDLSCs. Acquisition of a large number of PDLSCs is required for clinical application to widespread PDL destruction, which remains quite difficult.

In 2006, Takahashi and Yamanaka reprogramed somatic cells by forced expression of the transcription factors *Oct4*, *Klf4*, *Sox2*, and *c-Myc* [9]. The reprogramed cells acquired properties like those of embryonic stem cells (ESCs) including cell morphology, pluripotency, marker expression, and high proliferative capacity.

These cells were named induced pluripotent stem cells (iPSCs) based on their characteristics. Because they can be generated from individual somatic cells, iPSCs have the advantage of limited immune rejection upon autologous transplantation. Moreover, these cells overcome ethical issues associated with isolating human ESCs from blastocysts. Therefore, iPSCs have revolutionized the field of personalized medical research, such as *in vitro* disease modeling, drug screening, and regenerative cell therapy.

Variety types of somatic cells such as neural cells [10], kidney cells [11], cardiomyocytes [12], retinal pigment epithelial cells [13], intestinal epithelial cells [14], and blood cells [15] have been generated from iPSCs. We also developed a protocol to induce the differentiation of human iPSCs into PDLSC-like cells (iPDLSCs) exhibiting high expression of genes strongly expressed in PDLSCs including *COL1*, *FBN1*, *OPG*, and *POSTN* [16]. iPDLSCs also display high proliferative potential, mesenchymal stem cell-related marker expression, and mesenchymal-lineage (osteoblasts and adipocytes) differentiation potential. Therefore, iPDLSCs closely resemble PDLSCs and could become a promising cell source for regenerative cell therapy of PDL tissue.

Extracellular matrix (ECM), consisting of a large and varied group of macromolecules and their regulatory factors, is involved in tissue development, homeostasis, repair, and regeneration by regulating cell differentiation, migration, proliferation, apoptosis, and morphology [17] [18]. iPDLSCs are generated from iPSC-derived neural crest cells (iNCs) by culturing these cells on ECM derived from human PDL cells [16]. To improve the efficiency of this process, it is necessary to identify ECM components that more effectively differentiate iNCs into iPDLSCs. However, PDL cells have the ability to produce various types of ECM such as collagen, fibronectin, proteoglycan, osteopontin, bone sialoprotein, and osteonectin [19] [20] [21] [22]. Moreover, the composition of ECM varies depending on factors such as sex, age, and the type of tissue [23]. ECM derived from human PDL cells is heterogeneous and its function is wide-ranging and complicated; therefore, it is difficult to isolate one crucial component for inducing iPDLSCs from iNCs.

Transcription factors regulate the expression of various genes by directly binding specific DNA sequences located in gene promoters and distal regulatory elements [24]; therefore, they are considered to engage a variety of important biological responses. Previous publications demonstrated that various transcription factors such as SMAD3, Sp1, STAT5, Egr-1, and Nrf2 have the ability to interact with the promoters of ECM-related genes and regulate their expression [25] [26] [27] [28] [29]. Additionally, AP1 [30] and Mkx [31] can reportedly act as regulators of ECM-related gene expression in PDL cells. However, the transcription factors that regulate ECM production in human PDL cells – an important factor for differentiation of iNCs into iPDLSCs – have not been clarified. Given these hallmarks, we aimed to isolate the transcription factor responsible for generation of iPDLSCs by gene expression analysis and gene ontology (GO) enrichment analysis techniques using human PDL cells and dermal fibroblasts.

Materials And Methods

Cell culture

Human dermal fibroblasts (HDFs) and human iPSCs were purchased from RIKEN (Ibaraki, Japan; HPS No. RCB0156 and No. 0063). Human iPSCs were cultured on mouse embryonic fibroblasts (MEFs; ReproCELL, Kanagawa, Japan) and maintained in primate ESC medium (ReproCELL) containing 5 ng/mL human

recombinant basic fibroblast growth factor (b-FGF; ReproCELL) at 37℃ in a humidified atmosphere of 5% CO_2 and 95% air. Two human PDL cell populations were isolated from the third molar of a healthy 25-year-old female patient (HPDLC-3U) and 23-year-old male patient (HPDLC-3S), who visited Kyushu University for extraction, as described previously [32]. Informed consent was obtained from both tissue donors according to the guidelines of the Research Ethics Committee of Kyushu University Certified Institutional Review Board for Clinical Trials. HDF and HPDLCs were maintained in alpha-Minimum Essential Medium (α-MEM; Gibco-BRL, Grand Island, NY) supplemented with 50 U/μL penicillin and 50 μg/mL streptomycin (Wako, Osaka, Japan) containing 10% fetal bovine serum (FBS; Sigma-Aldrich, St. Louis, MO) (10% FBS/α-MEM) at 37℃ in a humidified atmosphere of 5% CO_2 and 95% air. All procedures were carried out following the rules of the Declaration of Helsinki and performed in compliance with the Research Ethics Committee of Kyushu University Certified Institutional Review Board for Clinical Trials. (Approval No. 2-115). We confirm that all experiments were performed in according to relevant guidelines and regulations.

Quantitative reverse transcription polymerase chain reaction

Total RNA was isolated from each cells using TRIzol Reagent (Invitrogen, Carlsbad, CA), and first-strand cDNA was removed from 500 ng of total RNA with an ExScript RT Reagent kit (Takara Bio, Kusatsu, Japan) according to the manufacturer's instructions. Quantitative RT-PCR assays were carried out using KAPA SYBR Fast qPCR kit (Nippon Genetics, Tokyo, Japan) in a Thermal Cycler Dice Real-Time System (Takara Bio) according to the manufacturer's instructions as described previously [16]. Specific primer sequences, GenBank ID, product sizes, and annealing temperatures for each gene are listed in Table 1. *β-actin* was used as an internal control in all quantitative RT-PCR. The expression levels of target genes were determined using the $2^{-\Delta\Delta Ct}$ method. Primer sequences were designed using the GenBank database (NCBI), and primer specificity was confirmed by GenBank BLAST searches.

Table 1
GenBank ID, primer sequences, product sizes, and annealing temperatures for quantitative reverse transcription polymerase chain reaction

Target gene (abbreviation)	GenBank ID	Forward (top) and reverse (bottom) primer sequences	Size of amplified products (bp)	Annealing temperature (°C)
b-actin	NM_001101.5	5'-ATTGCCGACAGGATGCAGA-3'/ 5'-GAGTACTTGCGCTCAGGAGGA-3'	89	60
Alpha smooth muscle actin (aSMA)	NM_001613.4	5'-GACAATGGCTCTGGGCTCTGTA-3'/ 5'-CTGTGCTTCGTCACCCACGTA-3'	147	60
Osteoprotegerin (OPG)	NM_002546.4	5'-CTCGAAGGTGAGGTTAGCATGTC-3'/ 5'-TGGCACCAAAGTAAACGCAGAG-3'	196	60
Alkaline phosphatase (ALP)	NM_001177520.3	5'-GGACCATTCCCACGTCTTCAC-3'/ 5'-CCTTGTAGCCAGGCCCATTG-3'	137	60
Periostin (POSTN)	NM_006475.2	5'-CATTGATGGAGTGCCTGTGGA-3'/ 5'-CAATGAATTTGGTGACCTTGGTG-3'	167	60
Type1 collagen (COL1a1)	NM_000088.3	5'-CCCGGGTTTCAGAGACAACTTC-3'/ 5'-TCCACATGCTTTATTCCAGCAATC-3'	148	60
Periodontal ligament-associated protein 1 (PLAP1)	NM_017680.5	5'-ATGGGAGTCTTGCTAACATACCAC-3'/ 5'-CAGAAGTCATTTACTCCCACTCTTG-3'	154	60
Forkhead box F2 (FOXF2)	NM_001452.2	5'-TCGCCTTACCTCAAGCAGC-3'/ 5'-AGAGTGATGCTGGTAACGGG-3'	165	60
SIX homeobox 2 (SIX2)	NM_016932.5	5'-GGCCGAGGCCAAGGAA-3'/ 5'-GGGCTGGATGATGAGTGGTC-3'	144	60
Distal-less homeobox 5 (DLX5)	NM_005221.6	5'-CAGAAGACTCAGTACCTCGCC-3'/ 5'-GTTACACGCCATTGGGTCG-3'	180	60

Target gene (abbreviation)	GenBank ID	Forward (top) and reverse (bottom) primer sequences	Size of amplified products (bp)	Annealing temperature (°C)
Paired box 9 (PAX9)	NM_001372076.1	5'-GCAGGAAGCCAAGTACGGT-3'/ 5'-TGTCACAGTTGTGGGGAGAC-3'	200	60
Transcription factor AP-4 (TFAP4)	NM_003223.3	5'-CACATCCCGGCAAAATCTGG-3'/ 5'-CCATGGCGTCACTGTCTGAG-3'	185	60
Osteocalcin (OCN)	NM_199173.4	5'-CCCAGGCGCTACCTGTATCAA-3'/ 5'-GGTCAGCCAACTCGTCACCAGTC-3'	112	60
Bone morphogenetic protein 2 (BMP2)	NM_001200.2	5'-TCCACTAATCATGCCATTGTTCAGA-3'/ 5'-GGGACACAGCATGCCTTAGGA-3'	73	60
Bone sialoprotein (BSP)	MN_004967.3	5'-CTGGCACAGGGTATACAGGGTTAG-3'/ 5'-ACTGGTGCCGTTTATGCCTTG-3'	181	60
Lipoprotein lipase (LPL)	NM_000237.2	5'-GACTCGTTCTCAGATGCCCT-3'/ 5'-ACTTCAGGCAGAGTGAATGGG-3'	145	60
Adiponectin (ADIPOQ)	NM_001177800.2	5'-CAGGAAACCACGACTCAAGGG-3'/ 5'-CCGGTTTCACCGATGTCTCC-3'	200	60
Leptin (LEP)	NM_000230.3	5'-GCTGTGCCCATCCAAAAAGTC-3'/ 5'-CCAGTGTCTGGTCCATCTTGG-3'	178	60
CCAAT enhancer binding protein alpha (CEBPa)	NM_004364.4	5'-GGTGGACAAGAACAGCAACGA-3'/ 5'-GTCATTGTCACTGGTCAGCTC-3'	136	60
Proliferator-activated receptor gamma (PPARg)	NM_138712.5	5'-TATTCTCAGTGGAGACCGCC-3'/ 5'-TGAGGACTCAGGGTGGTTCA-3'	115	60
Kruppel like factor 15 (KLF15)	NM_014079.4	5'-TACACCAAAAGCAGCCACCTC-3'/ 5'-CTGGTACGGCTTCACACCTG-3'	153	60

Differentiation of iPSC-derived neural crest cells (iNCs) cultured on ECM derived from HDF, HPDLC-3S, or HPDLC-3U

Human iPSCs were first differentiated into iNCs according to a previous report [33]. Briefly, separated human iPSCs were cultured on Matrigel-coated dishes with MEF-conditioned medium supplemented with 10 mM Rho-associated protein kinase inhibitor (Enzo Life Sciences, Farmingdale, NY) and 10 ng/mL b-FGF. After the cultures reached subconfluence, cells were cultured in neural crest cell differentiation medium composed of KnockOut DMEM (Gibco-BRL) supplemented with 15% KnockOut Serum Replacement, 1% L-glutamine, 1% non-essential amino acids, 50 U/mL penicillin, 50 mg/mL streptomycin, 0.1% 2-mercaptoethanol (Sigma-Aldrich), 500 ng/mL Noggin (PeproTech, Inc., Rocky Hill, NJ), and 10 mM SB431542 (Tocris, Minneapolis, MN) according to culture periods. Following of 10 days incubation, cells were subjected to magnetic-activated cell sorting (Miltenyi Biotec, Bergisch Gladbach, Germany) using a bead-conjugated p75NTR antibody (Miltenyi Biotec) for the isolation of iNCs. HDF, HPDLC-3S, and HPDLC-3U cells were separately cultured in 10% FBS/α-MEM until reaching confluency and then detached with 2% EDTA (Nacalai Tesque, Kyoto, Japan) in phosphate-buffered saline (PBS) to obtain dishes coated with ECM. iNCs were seeded on these ECM-coated dishes and further cultured for 2 weeks. Following culture, iNCs exposed to ECM derived from HDF, HPDLC-3S, and HPDLC-3U were named iNC-HDF, iNC-3S, and iNC-3U, respectively.

Cap analysis gene expression and gene ontology enrichment analysis

Cap analysis of gene expression (CAGE) allows genome-wide analysis of gene transcription start sites and quantitative study of RNA transcribed from them by DNAFORM (Yokohama, Kanagawa, Japan). In brief, RNA quality was assessed with a Bioanalyzer (Agilent, Santa Clara, CA) to ensure that the RNA integrity number was over 7.0, and A260/280 and 260/230 ratios were over 1.7. First-strand cDNAs were transcribed to the 5′ end of capped RNAs and attached to CAGE “barcode” tags, which upon sequencing were mapped to the mouse mm9 genomes using BWA software (v0.5.9) after discarding ribosomal or non-A/C/G/T base-containing RNAs. For tag clustering, CAGE-tag 5′ coordinates were input for CAGEr clustering using 20 bases as a maximal allowed distance between two neighboring tags and a minimum counts per million (CPM) value of 2 [34]. GO enrichment analysis was also performed using BWA and Gene Set Enrichment Analysis (GSEA) software [35] [36].

Small interfering RNA transfection

Small interfering RNA (siRNA) for human *PAX9* (MISSION siRNA, SASI_Hs02_00341076; Sigma-Aldrich) or human control siRNA (MISSION siRNA Universal Negative Control #1, SIC-001-10; Sigma-Aldrich) were introduced into HPDLC-3U using Lipofectamine RNAiMAX (Invitrogen) according to the manufacturer’s instructions as described previously [37]. Briefly, HPDLC-3U cells were seeded in 24-well plates (Becton Dickinson Labware, Lincoln Park, NJ) at a density of 1×10^4 cells per well in Opti-MEM (Invitrogen) containing 10% FBS. After they reached 50–70% confluency, siRNA were transduced. The siRNA-lipid complex was prepared by mixing 10 pmol siRNA and 1.5 μL of Lipofectamine RNAiMAX in 50 μL Opti-MEM. The complex was incubated for 5 min at room temperature, then added to cells and the mixture was incubated for 48 h. HPDLC-3U transfected with control siRNA and PAX9 siRNA were designated 3U + siCont and 3U + siPAX9, respectively. Untransfected HPDLC-3U was designated Unt-3U.

Differentiation of iPSC-derived neural crest cells (iNCs) cultured on ECM derived from Unt-3U, 3U + siCont, and 3U + siPAX9

Unt-3U, 3U + siCont, and 3U + siPAX9 were cultured in 10% FBS/α-MEM until reaching confluency. Subsequently, cells were detached with 2% EDTA in PBS and then iNCs were seeded on these ECM-coated dishes and cultured for 2 weeks. iNCs exposed to ECM derived from Unt-3U, 3U + siCont, and 3U + siPAX9 were designated iNC-Unt, iNC-siCont, and iNC-siPAX9, respectively.

Immunofluorescence staining

iNC-Unt, iNC-siCont, and iNC-siPAX9 were fixed with 4% paraformaldehyde (Nacalai Tesque) and 0.5% dimethyl sulfoxide (Nacalai Tesque) in PBS for 30 min. 2% bovine serum albumin in PBS was used to blocking cells for 1 h and then cells were incubated with rabbit polyclonal anti-human OPG (5 μg/mL; Abcam, Cambridge, UK), rabbit polyclonal anti-human POSTN antibody (1:100 dilution; Sigma-Aldrich), or rabbit polyclonal IgG isotype control antibody (Cell Signaling Technology, Beverly, MA) overnight at 4°C. The following day, cells were washed three times with PBS and incubated with an Alexa Fluor 647-conjugated chicken anti-rabbit antibody (1:250 dilution; Invitrogen). After 1 h, the cells were washed three times with PBS and counterstained with DAPI (Nacalai Tesque). Stained cells were imaged and analyzed using a Biozero digital microscope (Keyence Corporation, Osaka, Japan).

Flow cytometric analysis

iNC-Unt, iNC-siCont, and iNC-siPAX9 were detached with Accutase (ReproCELL) and adjusted to a density of 5×10^5 cells/tube. Next, cells were incubated with R-phycoerythrin-conjugated mouse anti-human CD 34, CD45, CD90, CD105, CD166 (BioLegend, San Diego, CA), IgG1, or IgG2a (iCyte, Tokyo, Japan) for 45 min at 4°C. Cells were then washed with flow cytometry buffer (R&D Systems, Minneapolis, MN) and percentages of positive cells were measured by flow cytometry (EC800 Cell Analyzer; Sony, Tokyo, Japan). Data were analyzed using Eclipse software (Sony).

Proliferation assay

iNC-Unt, iNC-siCont, and iNC-siPAX9 were seeded at a density of 3×10^3 cells/well into wells of 48-well plates and incubated for up to 7 days. Subsequently, their proliferation was examined using a cell proliferation assay kit (Takara Bio) on 0, 1, 2, 3, 5, and 7 days. After incubation, 25 μL of the WST-1 kit reagent was added to the culture medium of each well. Following 1 h of treatment, 100 μL of supernatant was collected from each well, and the optical density at 450 nm of each well was measured with an iMark microplate reader (Bio-Rad Laboratories).

Osteoblastic differentiation

iNC-HDF, iNC-3S, iNC-3U, iNC-Unt, iNC-siCont, and iNC-siPAX9 were seeded at a density of 2×10^4 cells into wells of a 24-well plate and cultured in 10% FBS/α-MEM (control medium; CM). After reaching confluence, the culture medium was changed to an osteoblastic differentiation medium (ODM) composed of CM supplemented with 50 μg/mL ascorbic acid (Nacalai Tesque) and 2 mM β-glycerophosphate (Sigma Aldrich). As a control, cells were cultured in CM. After 3 weeks of culture, cells were fixed with 10% formalin (Wako) for 1 h, washed with distilled water, and stained with 0.3% Alizarin Red S (Invitrogen) as described previously [16]. Images of stained cell were captured with a Keyence BZ-9000 microscope (Osaka, Japan).

Nine fields were randomly chosen for quantification of Alizarin Red S-positive area. Measurements were performed using BZ-X Analyzer Software (Keyence).

Adipocytic differentiation

iNC-HDF, iNC-3S, iNC-3U, iNC-Unt, iNC-siCont, and iNC-siPAX9 were seeded at a density of 2×10^4 cells into wells of a 24-well plate and cultured in CM. After reaching confluence, the culture medium was changed to an adipocytic differentiation medium (ADM) composed of CM supplemented with 1% L-glutamine, 0.1 mM L-ascorbic acid (Wako), 1 mM Sodium Pyruvate Solution (100×, Nacalai Tesque), 10 μM hydroxyethyl-piperazinyl ethanesulfonic acid (Nacalai tesque), 60 mM indomethacin (Sigma-Aldrich), and 10^{-7} M dexamethasone (Merck Millipore, Darmstadt, Germany). As a control, cells were cultured in CM. After 4 weeks, cells were fixed with 10% formalin, washed with distilled water, and stained with 0.3% Oil Red O (Invitrogen) for lipid detection as described previously [16]. Images of stained cell were captured with a Keyence BZ-9000 microscope. Nine fields were randomly chosen for quantification of the number of Oil Red O-positive cells.

Statistical analysis

All values are expressed as the mean ± standard deviation. Statistical analysis was performed using one-way ANOVA, followed by the Bonferroni method for comparisons of three or more groups. P values of < 0.05 were considered statistically significant.

Results

Periodontal ligament stem cell characteristics of iNC-HDF, iNC-3S, and iNC-3U

HDFs, HPDLC-3S cells, and HPDLC-3U cells showed typical fibroblastic morphologies, namely plump spindle or stellate shapes with centrally placed round nuclei (Fig. 1A). HPDLC-3S and HPDLC-3U cells highly expressed PDL-related genes *αSMA*, *OPG*, and *ALP* compared with HDFs (Fig. 1B). iNC-HDF mainly exhibited rounded shapes (Fig. 1C[I]), while iNC-3S included cells with round or spindle shapes (Fig. 1C[II]). iNC-3U was mainly comprised of spindle-shaped cells (Fig. 1C[III]). As with our previous study [16], iNC-3U displayed higher expression of iPDLSC-associated genes *OPG*, *POSTN*, *COL1A1*, and *PLAP1* compared with HDF (Fig. 1D). iNC-3S also increased their expression compared with HDF (Fig. 1D). Additionally, expression of *OPG*, *COL1A1*, and *PLAP1* was upregulated in iNC-3U compared with iNC-3U (Fig. 1D). After osteoblastic induction, iNC-HDF formed small number of Arizarin Red S-positive mineralized deposits (Fig. 1E[I]), while iNC-3S generated more mineralized deposits than iNC-HDF (Fig. 1E[II]). iNC-3U formed large numbers of mineralized deposits compared with iNC-HDF and iNC-3S (Fig. 1E[III]). Following adipocytic induction, iNC-HDF formed no Oil Red O-positive lipid droplets (Fig. 1F[I]) and iNC-3S generated only a small number of lipid droplets (Fig. 1F[II]). In contrast, iNC-3U formed large numbers of lipid droplets compared with iNC-HDF and iNC-3S (Fig. 1F[III]).

Identification of transcription factor genes highly expressed in HPDLC-3U

Expression levels of iPDLSC-related genes and their ability to differentiate into osteoblasts and adipocytes varied between iNC-HDF, iNC-3S, and iNC-3U. Therefore, we performed CAGE to compare gene expression among HDF, HPDLS-3S, and HPDLC-3U. A total of 13728 genes were screened out (Fig. 2A), of which 1986

were upregulated in HPDLC-3S by > 2-fold relative to HDF. GO analysis indicate that the term “DNA binding transcriptional activator activity” was enriched in HPDLC-3S compared with HDF, and 15 genes were included in this term (Fig. 2B). Among them, expression of five genes (*FOXF2*, *SIX2*, *DLX5*, *PAX9*, and *TFAP4*) was upregulated in HPDLC-3U relative to HPDLC-3S. GSEA confirmed that these genes played various roles not only in regulation of transcription, but also compound metabolic processes, cellular biosynthetic processes, and animal organ morphogenesis (Fig. 2C). Quantitative RT-PCR analysis performed to investigate their expression in HDF, HPDLC-3S, and HPDLC-3U showed that expression of all fives genes was significantly higher in HPDLC-3S than in HDF (Fig. 2D). Expression of these genes was also significantly higher in HPDLC-3U than in HDF; however, expression of *SIX2*, *DLX5*, and *TFAP4* showed no difference between HPDLC-3S and HPDLC-3U (Fig. 2D). Moreover, *FOXF2* and *PAX9* expression was significantly higher in HPDLC-3U than in HPDLC-3S (Fig. 2D). Further comparison of their expression levels in HPDLC-3S and HPDLC-3U revealed that the rate of increase was higher for *PAX9* than *FOXF2* (Fig. 2D). On the basis of these analyses, we focused on *PAX9* in this study.

PAX9 gene expression in Unt-3U, 3U + siCont, and 3U + siPAX9

To evaluate the effect of *PAX9* on the ability of ECM derived from HPDLC-3U to induce differentiation of iNCs into iPDLSCs, we transfected si-PAX9 into HPDLC-3U to downregulate PAX9 expression. *PAX9* expression was significantly decreased in 3U-siPAX9 compared with Unt-3U and 3U-siCont (Fig. 3A). However, Unt-3U, 3U + siCont, and 3U + siPAX9 revealed typical fibroblastic shapes and almost identical morphologies (Fig. 3B).

iPDLSC-associated marker expression in iNC-Unt, iNC-siCont, and iNC-siPAX9

Next, we generated iNC-Unt, iNC-siCont, and iNC-siPAX9 by culturing iNCs on Unt-3U, 3U + siCont, and 3U + siPAX9 for 2 weeks, respectively (Fig. 3C). iNC-Unt, iNC-siCont, and iNC-siPAX9 exhibited spindle shapes and did not include cells exhibiting rounded shapes (Fig. 3D[I–III]). Expression levels of *OPG*, *POSTN*, *COL1A1*, and *PLAP1* were almost identical between iNC-Unt and iNC-siCont (Fig. 3E). However, expression of these genes was significantly downregulated in iNC-siPAX9 compared with iNC-Unt and iNC-siCont (Fig. 3E). Moreover, many cells were positive for OPG and POSTN in iNC-Unt and iNC-siCont (Fig. 3F[I, II, V, VI]), while few cells showed positive reactions in iNC-siPAX9 (Fig. 3F[III, VII]). No staining was observed in iNC-Unt stained with control IgG (Fig. 3F[IV, VIII]).

Proliferation and cell surface marker expression in iNC-Unt, iNC-siCont, and iNC-siPAX9

iNC-Unt, iNC-siCont, and iNC-siPAX9 exhibited a time-dependent increase in proliferation (Fig. 4A). iNC-Unt exhibited higher levels of proliferation than iNC-siCont and iNC-siPAX9 on days 2, 3, 5 and 7; however, there was no statistically significant difference in proliferation between iNC-Unt, iNC-siCont, or iNC-siPAX9 from days 1–7 (Fig. 4A). Cells highly expressed the MSC-associated surface markers CD90, CD105, and CD166, and slightly expressed the hematopoietic cell-associated markers CD34 and CD45 (Fig. 4B). Moreover, expression levels of MSC- and hematopoietic-associated markers were almost identical between iNC-Unt, iNC-siCont, and iNC-siPAX9 (Fig. 4B).

Osteoblastic differentiation of iNC-Unt, iNC-siCont, and iNC-siPAX9

After 3 weeks of culture in ODM, iNC-Unt, iNC-siCont, and iNC-siPAX9 formed large numbers of Alizarin Red S-positive mineralized deposits (Fig. 5A). Indeed, there was no statistically significant difference in Alizarin Red S-positive area between cultures (Fig. 5B). In contrast, no deposits were observed in iNC-Unt, iNC-siCont, and iNC-siPAX9 treated with CM (Supplement Fig. 1A[I–III]). Expression of osteoblast-related markers *OCN*, *BMP2*, and *BSP* was upregulated in iNC-Unt, iNC-siCont, and iNC-siPAX9 cultured in DM compared with cells cultured in CM (Fig. 5C), and were not statistically different between these groups (Fig. 5C).

Adipocytic differentiation of iNC-Unt, iNC-siCont, and iNC-siPAX9

After 4 weeks of culture in ADM, iNC-Unt and iNC-siCont formed large number of lipid droplets, while iNC-siPAX9 generated only a small number of lipid droplets (Fig. 6A). Indeed, there were statistically significant differences in numbers of cells exhibiting lipid droplets between iNC-Unt and iNC-siPAX9, and iNC-siCont and iNC-siPAX9 (Fig. 6B). In contrast, no droplets were observed in cells treated with CM (Supplement Fig. 1B[I–III]). Expression of adipocyte-related markers *LPL*, *ADIPOQ*, and *LEP* was upregulated in iNC-Unt, iNC-siCont, and iNC-siPAX9 cultured in ADM compared with cells cultured in CM (Fig. 6C). Moreover, their expression was downregulated in iNC-siPAX9 cultured in ADM compared with iNC-Unt and iNC-siCont cultured in ADM (Fig. 6C). Expression of regulator genes for adipogenesis (*CEBPa, PPARg*, and *KLF15*) was also suppressed in iNC-siPAX9 cultured in ADM relative to iNC-Unt and iNC-siCont cultured in ADM (Fig. 6D).

Discussion

iNCs require culture on ECM derived from human PDL cells to differentiate into iPDLSCs [16]. Therefore, human PDL cell-derived ECM plays important roles in the generation of iPDLSCs. The morphology, iPDLSC-associated gene expression, and mesenchymal lineage cell differentiation of iNCs cultured on ECM derived from HPDLC-3S varied from cells cultured on ECM derived from HPDLC-3U, although both HPDLC-3S and HPDLC-3U were human PDL cells. HPDLCs were isolated from different individuals (HPDLC-3S: 23-year-old male, HPDLC-3U: 25-year-old female) and some factors, such as sex and age, can reportedly affect the composition of ECM [23]. CAGE results also demonstrated that gene expression patterns of HPDLC-3S and HPDLC-3U were different to some extent; specifically, 693 genes were upregulated and 675 genes were downregulated in HPDLC-3U by > 2-fold relative to HPDLC-3S. These results indicate that differences in the composition of ECM between HPDLC-3S and HPDLC-3U likely cause of the observed difference in their ability to induce iPDLSCs from iNCs.

Our previous study demonstrated that iNCs cultured with the major components of ECM in human PDL cells, COL1 and POSTN, displayed lower expression of iPDLSC-associated genes relative to iPDLSCs. Moreover, our previous report revealed that artificially isolated single ECM components were insufficient to mimic the complex structure and complete function of natural ECM [38]. Therefore, we aimed to identify the transcription factor regulating the production of ECM in human PDL cells, which is responsible for the induction of iNCs to iPDLSCs. We focused on the transcription factor *PAX9* on the basis of results from CAGE and GSEA technologies. PAX9 belongs to the paired box family that encodes a group of growth- and development-regulation-related transcription factors [39]. GSEA results also indicated the involvement of *PAX9* in head morphogenesis, body morphogenesis, face development, tissue development, and regulation of animal organ morphogenesis. PAX9 expression was previously confirmed in various tissues such as

thymus, parathyroid, tonsil, vagina, and cervix [40] [41]. Its expression was also identified in oral tissues including salivary glands, taste papilla of the tongue, lip, and developing palatal shelves [42]. Moreover, Pax9 is widely expressed in dental mesenchyme of developing tooth germ, whereby defects in Pax9 were associated with a lack of tooth buds and hypodontia [43]. Dental mesenchyme cells, which originate from neural crest cells, produce PDLSCs that ultimately form PDL tissue [3]; therefore, PAX9 is suggested to be a crucial factor regulating the differentiation of neural crest cells into PDLSCs.

PAX9 reportedly regulates some ECM genes; for example, exogenous *PAX9* increases expression of dentin matrix protein 1 in human iNCs [44], while endogenous Pax9 positively regulates *Col2a1* and *Acan* in mouse prechondrogenic mesenchymal cells of the intervertebral discs [45]. Additionally, several studies demonstrated the effects of ECM on multipotency of stem cells. Kearns et al. suggested that the ECM environment of the central nervous system is crucial for the maintenance of multipotency of neural stem cells [46],while Antoon et al. revealed that bladder-derived ECM was of great importance to maintain the multipotency in MSCs [47]. Interestingly, tendon stem/progenitor cells contacting ECM derived from the tendon of $Bgn^{-/0}Fmod^{-/-}$ mice exhibited lower potential to differentiate into tenocytes compared with cells contacting ECM derived from wild-type mice [48]. These results strongly support our finding that ECM derived from 3U-siPAX9 impaired expression of iPDLSC-associated markers and the differentiation of adipocytes by iNCs. However, cell morphology, proliferation, surface marker expression, and osteoblastic differentiation did not vary between iNC-Unt3U, iNC-siCont, and iNC-siPAX9, suggesting that *PAX9* partially regulates ECM production in human PDL cells although other transcription factors are likely involved. As with *PAX9*, *FOXF2* expression was significantly higher in HPDLC-3U compared with HDF and HPDLC-3S. GENE MANIA analysis demonstrated co-expression of *PAX9* with *FOXF2* (Supplement Fig. 2A). FOXF2 is a specific mesenchymal transcription factor expressed in mesenchymal cells adjacent to the epithelium [49]. Ormestad et al. demonstrated that *Foxf2* promotes ECM synthesis in fibroblasts to support mouse gut development [50]. $Foxf2^{-/-}$ mice develop a cleft palate because of defects in ECM synthesis of the secondary palate [51]; intriguingly, this phenotype is consistent with that of *PAX9*-deficient mice exhibiting a cleft secondary palate at birth [42]. Collectively, these results indicate that FOXF2 may also be involved in the differentiation of iNCs into iPDLSCs via regulation of ECM synthesis in human PDL cells. Additionally, GENE MANIA analysis indicated physical interactions, co-expression, and co-localization of *PAX9* with transcription factor genes such as *MSX1*, *PAX2*, *PAX3*, *PAX4*, *PAX6*, and *PAX7* (Supplement Fig. 2B). Among them, only the interaction between *PAX9* and *MSX1* has been clarified. Vieira et al. tested for possible *PAX9-MSX1* interactions by observing the transmission of marker alleles from parents, suggesting that *PAX9* interacts with *MSX* to cause tooth agenesis in humans [52]. Ogawa et al. further demonstrated that their interaction regulated *Bmp4* expression to determine the fate of the transition from bud stage to cap stage during tooth development [53]. CAGE results revealed slightly increased *MSX1* expression in HPDLC-3U relative to HDF (1.72-fold) and HPDLC-3S (1.12-fold) (data not shown). Therefore, further studies are essential to identify the interaction between *PAX9* and *MSX1*, and their involvement in regulation of ECM synthesis in PDL cells.

In summary, we compared the ability of ECM derived from HDF, HPDLC-3S, and HPDLC-3U to induce differentiation of iNCs into iPDLSCs. iNCs cultured on ECM derived from HPDLC-3U displayed PDLSC-like phenotypes (Fig. 7) and strong expression of *PAX9* compared with HDF and HPDLC-3S. siPAX9 transfection successfully downregulated PAX9 at gene and protein levels in HPDLC-3U. iNCs cultured on ECM derived

from siPAX9-transfected HPDLC-3U exhibited decreased expression of iPDLSC-associated markers and adipocyte differentiation ability (Fig. 7). We report the involvement of *PAX9* in regulation of ECM production in human PDL cells, which plays important roles in the differentiation of iNCs into iPDLSCs. *PAX9* may be an effective marker for selecting human PDL cells that produce ECM responsible for the generation of iPDLSCs. Moreover, human PDL cells highly expressing *PAX9* may contribute to the progress of regenerative medicine for PDL tissues via efficient induction of iNCs to iPDLSCs by their ECM.

Declarations

Data availability

CASE analysis data generated and/or analyzed during the current study are available in the Gene Expression Omnibus (GEO) repository, Accession Number GSE208250. The other datasets either generated and analyzed or just analyzed in this study are available from the corresponding author upon reasonable request.

Acknowledgments

We thank Drs. Obata, Itoyama, Ono, Ipposhi, Kaneko, Safwan, Anas, and Tashita for their great support in the preparation of this work. We thank Amy Van Deusen, Ph.D., from Edanz (https://jp.edanz.com/ac) for editing a draft of this manuscript.

Authors' Disclosure Statement

A.T., S.H., and H.M proposed the idea and conceived the experiments, A.T. and S.H. conducted the experiments, D.H., S.Y., H.S., S.F., O.A., M.K., and D.Y. supported the experiments, S.H., A.T., D.H., S.Y., H.S., S.F., and H.M. analyzed the results. All authors reviewed the manuscript. The authors have no conflict of interest directly relevant to the content of this article.

Funding Information

Funding: This work was financially supported by Grants-in-Aid for Scientific Research (Project Nos. JP17H01598, JP18K19651, JP21K09876, JP21K19608, and JP22H03271) from the Japan Society for the Promotion of Science.

References

1. Carnes, D.L., C.L. Maeder, and D.T. Graves, Cells with osteoblastic phenotypes can be explanted from human gingiva and periodontal ligament. *J Periodontol.* 1997. **68**(7): p. 701-7.
2. Tomokiyo, A., et al., Development of a multipotent clonal human periodontal ligament cell line. *Differentiation.* 2008. **76**(4): p. 337-47.
3. Seo, B.M., et al., Investigation of multipotent postnatal stem cells from human periodontal ligament. *Lancet.* 2004. **364**(9429): p. 149-55.
4. Wada, N., et al., Immunomodulatory properties of human periodontal ligament stem cells. *J Cell Physiol.* 2009. **219**(3): p. 667-76.

5. Liu, D., et al., Mesenchymal stem cells derived from inflamed periodontal ligaments exhibit impaired immunomodulation. *J Clin Periodontol.* 2012. **39**(12): p. 1174-82.
6. Liu, O., et al., Periodontal ligament stem cells regulate B lymphocyte function via programmed cell death protein 1. *Stem Cells.* 2013. **31**(7): p. 1371-82.
7. Shin, C., et al., Human periodontal ligament stem cells suppress T-cell proliferation via down-regulation of non-classical major histocompatibility complex-like glycoprotein CD1b on dendritic cells. *J Periodontal Res.* 2017. **52**(1): p. 135-146.
8. Shalini, H.S. and K.L. Vandana, Direct application of autologous periodontal ligament stem cell niche in treatment of periodontal osseous defects: A randomized controlled trial. *J Indian Soc Periodontol.* 2018. **22**(6): p. 503-512.
9. Takahashi, K. and S. Yamanaka, Induction of pluripotent stem cells from mouse embryonic and adult fibroblast cultures by defined factors. *Cell.* 2006. **126**(4): p. 663-76.
10. Denham, M. and M. Dottori, Neural differentiation of induced pluripotent stem cells. *Methods Mol Biol.* 2011. **793**: p. 99-110.
11. Tsujimoto, H., et al., A Modular Differentiation System Maps Multiple Human Kidney Lineages from Pluripotent Stem Cells. *Cell Rep.* 2020. **31**(1): p. 107476.
12. Karakikes, I., et al., Human induced pluripotent stem cell-derived cardiomyocytes: insights into molecular, cellular, and functional phenotypes. *Circ Res.* 2015. **117**(1): p. 80-8.
13. Sun, J., et al., Protective Effects of Human iPS-Derived Retinal Pigmented Epithelial Cells in Comparison with Human Mesenchymal Stromal Cells and Human Neural Stem Cells on the Degenerating Retina in rd1 mice. *Stem Cells.* 2015. **33**(5): p. 1543-53.
14. Takayama, K., et al., Generation of Human iPSC-Derived Intestinal Epithelial Cell Monolayers by CDX2 Transduction. *Cell Mol Gastroenterol Hepatol.* 2019. **8**(3): p. 513-526.
15. El Hokayem, J., H.N. Cukier, and D.M. Dykxhoorn, Blood Derived Induced Pluripotent Stem Cells (iPSCs): Benefits, Challenges and the Road Ahead. *J Alzheimers Dis Parkinsonism.* 2016. **6**(5).
16. Hamano, S., et al., Extracellular Matrix from Periodontal Ligament Cells Could Induce the Differentiation of Induced Pluripotent Stem Cells to Periodontal Ligament Stem Cell-Like Cells. *Stem Cells Dev.* 2018. **27**(2): p. 100-111.
17. Lu, P., et al., Extracellular matrix degradation and remodeling in development and disease. *Cold Spring Harb Perspect Biol.* 2011. **3**(12).
18. Bonnans, C., J. Chou, and Z. Werb, Remodelling the extracellular matrix in development and disease. *Nat Rev Mol Cell Biol.* 2014. **15**(12): p. 786-801.
19. Ramakrishnan, P.R., et al., Synthesis of noncollagenous extracellular matrix proteins during development of mineralized nodules by rat periodontal ligament cells in vitro. *Calcif Tissue Int.* 1995. **57**(1): p. 52-9.
20. Worapamorn, W., et al., Cell surface proteoglycan expression by human periodontal cells. *Connect Tissue Res.* 2000. **41**(1): p. 57-68.
21. Tomokiyo, A., et al., Detection, Characterization, and Clinical Application of Mesenchymal Stem Cells in Periodontal Ligament Tissue. *Stem Cells Int.* 2018. **2018**: p. 5450768.

22. Tomokiyo, A., N. Wada, and H. Maeda, Periodontal Ligament Stem Cells: Regenerative Potency in Periodontium. *Stem Cells Dev.* 2019. **28**(15): p. 974-985.
23. McKee, T.J., et al., Extracellular matrix composition of connective tissues: a systematic review and meta-analysis. *Sci Rep.* 2019. **9**(1): p. 10542.
24. Latchman, D.S., Transcription factors: an overview. *Int J Biochem Cell Biol.* 1997. **29**(12): p. 1305-12.
25. Chen, S.J., et al., Interaction of smad3 with a proximal smad-binding element of the human alpha2(I) procollagen gene promoter required for transcriptional activation by TGF-beta. *J Cell Physiol.* 2000. **183**(3): p. 381-92.
26. Larouche, K., et al., Expression of the alpha 5 integrin subunit gene promoter is positively regulated by the extracellular matrix component fibronectin through the transcription factor Sp1 in corneal epithelial cells in vitro. *J Biol Chem.* 2000. **275**(50): p. 39182-92.
27. Rockel, J.S., S.M. Bernier, and A. Leask, Egr-1 inhibits the expression of extracellular matrix genes in chondrocytes by TNFalpha-induced MEK/ERK signalling. *Arthritis Res Ther.* 2009. **11**(1): p. R8.
28. Hiebert, P., The Nrf2 transcription factor: A multifaceted regulator of the extracellular matrix. *Matrix Biol Plus.* 2021. **10**: p. 100057.
29. Xu, R., V.A. Spencer, and M.J. Bissell, Extracellular matrix-regulated gene expression requires cooperation of SWI/SNF and transcription factors. *J Biol Chem.* 2007. **282**(20): p. 14992-9.
30. Kook, S.H., et al., Mechanical force induces type I collagen expression in human periodontal ligament fibroblasts through activation of ERK/JNK and AP-1. *J Cell Biochem.* 2009. **106**(6): p. 1060-7.
31. Takada, K., et al., Single Cell RNA Sequencing Reveals Critical Functions of Mkx in Periodontal Ligament Homeostasis. *Front Cell Dev Biol.* 2022. **10**: p. 795441.
32. Wada, N., et al., Periodontal ligament cells secrete the factor that inhibits osteoclastic differentiation and function: the factor is osteoprotegerin/osteoclastogenesis inhibitory factor. *J Periodontal Res.* 2001. **36**(1): p. 56-63.
33. Lee, G., et al., Derivation of neural crest cells from human pluripotent stem cells. *Nat Protoc.* 2010. **5**(4): p. 688-701.
34. Haberle, V., et al., CAGEr: precise TSS data retrieval and high-resolution promoterome mining for integrative analyses. *Nucleic Acids Res.* 2015. **43**(8): p. e51.
35. Mootha, V.K., et al., PGC-1alpha-responsive genes involved in oxidative phosphorylation are coordinately downregulated in human diabetes. *Nat Genet.* 2003. **34**(3): p. 267-73.
36. Subramanian, A., et al., Gene set enrichment analysis: a knowledge-based approach for interpreting genome-wide expression profiles. *Proc Natl Acad Sci U S A.* 2005. **102**(43): p. 15545-50.
37. Ipposhi, K., et al., Secreted Frizzled-Related Protein 1 Promotes Odontoblastic Differentiation and Reparative Dentin Formation in Dental Pulp Cells. *Cells.* 2021. **10**(9).
38. Xiong, X., et al., Extracellular matrix derived from human urine-derived stem cells enhances the expansion, adhesion, spreading, and differentiation of human periodontal ligament stem cells. *Stem Cell Res Ther.* 2019. **10**(1): p. 396.
39. Chen, X., et al., PAX9 in Cancer Development. *Int J Mol Sci.* 2022. **23**(10).

40. Peters, H., et al., Isolation of the Pax9 cDNA from adult human esophagus. *Mamm Genome.* 1997. **8**(1): p. 62-4.
41. Bannykh, S.I., et al., Aberrant Pax1 and Pax9 expression in Jarcho-Levin syndrome: report of two Caucasian siblings and literature review. *Am J Med Genet A.* 2003. **120a**(2): p. 241-6.
42. Peters, H., et al., Pax9-deficient mice lack pharyngeal pouch derivatives and teeth and exhibit craniofacial and limb abnormalities. *Genes Dev.* 1998. **12**(17): p. 2735-47.
43. Nakatomi, M., et al., Genetic interactions between Pax9 and Msx1 regulate lip development and several stages of tooth morphogenesis. *Dev Biol.* 2010. **340**(2): p. 438-49.
44. Seki, D., et al., Differentiation of Odontoblast-Like Cells From Mouse Induced Pluripotent Stem Cells by Pax9 and Bmp4 Transfection. *Stem Cells Transl Med.* 2015. **4**(9): p. 993-7.
45. Sivakamasundari, V., et al., A developmental transcriptomic analysis of Pax1 and Pax9 in embryonic intervertebral disc development. *Biol Open.* 2017. **6**(2): p. 187-199.
46. Kearns, S.M., et al., Extracellular matrix effects on neurosphere cell motility. *Exp Neurol.* 2003. **182**(1): p. 240-4.
47. Antoon, R., et al., Impact of bladder-derived acellular matrix, growth factors, and extracellular matrix constituents on the survival and multipotency of marrow-derived mesenchymal stem cells. *J Biomed Mater Res A.* 2012. **100**(1): p. 72-83.
48. Bi, Y., et al., Identification of tendon stem/progenitor cells and the role of the extracellular matrix in their niche. *Nat Med.* 2007. **13**(10): p. 1219-27.
49. Hupe, M., et al., Gene expression profiles of brain endothelial cells during embryonic development at bulk and single-cell levels. *Sci Signal.* 2017. **10**(487).
50. Ormestad, M., et al., Foxf1 and Foxf2 control murine gut development by limiting mesenchymal Wnt signaling and promoting extracellular matrix production. *Development.* 2006. **133**(5): p. 833-43.
51. Wang, T., et al., Forkhead transcription factor Foxf2 (LUN)-deficient mice exhibit abnormal development of secondary palate. *Dev Biol.* 2003. **259**(1): p. 83-94.
52. Vieira, A.R., et al., MSX1, PAX9, and TGFA contribute to tooth agenesis in humans. *J Dent Res.* 2004. **83**(9): p. 723-7.
53. Ogawa, T., et al., Functional consequences of interactions between Pax9 and Msx1 genes in normal and abnormal tooth development. *J Biol Chem.* 2006. **281**(27): p. 18363-9.

Figures

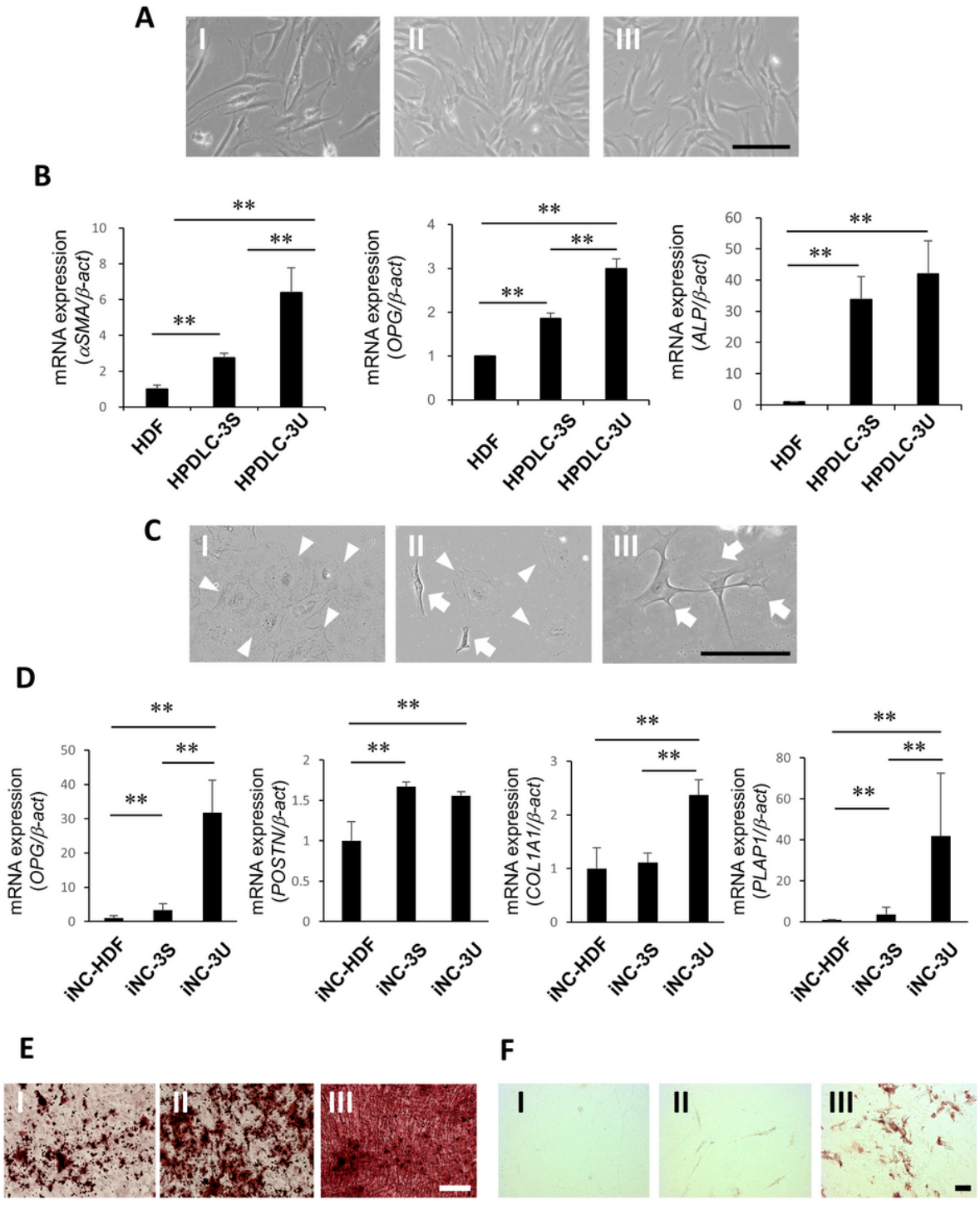

Figure 1

PDLSC characteristics of iNC-HDF, iNC-3S, and iNC-3U

A: Representative phase-contrast microscopic images of HDF (I), HPDLC-3S (II), and HPDLC-3U (III). Bar = 100 mm. B: Quantitative real time RT-PCR analysis of PDL-related genes *a-SMA*, *OPG*, and *AL,* in HDF, HPDLC-3S, and HPDLC-3U. b-act was used as an internal standard. Data shown are the mean ± standard deviation (n = 4). **P < 0.01. C: Representative phase-contrast microscopic images of iNC-HDF (I), iNC-3S (II), and iNC-

3U (III). White arrowheads indicate cells with rounded shapes and white arrows indicate cells with spindle shapes. Bar = 100 mm. D: Quantitative real-time RT-PCR analysis of iPDLSC-associated genes *OPG*, *POSTN*, *COL1A1*, and *PLAP1* in iNC-HDF, iNC-3S, and iNC-3U. b-act was used as an internal standard. Data shown are the mean ± standard deviation (n = 4). **P < 0.01. E: Representative Arizarn Red S-staining images of iNC-HDF (I), iNC-3S (II), and iNC-3U (III) after 3 weeks of culture in ODM. Bar = 100 mm. F: Representative Oil red O-staining images of iNC-HDF (I), iNC-3S (II), and iNC-3U (III) after 4 weeks of culture in ADM. Bar = 100 mm. HDF, human dermal fibroblasts; HDPLC, human periodontal ligament cell; iNC, neural crest-like cells derived from human induced pluripotent stem cells; iPDLSC, periodontal ligament stem cell-like cells derived from iNC; ODM, osteoblastic differentiation medium; ADM, adipocytic differentiation medium.

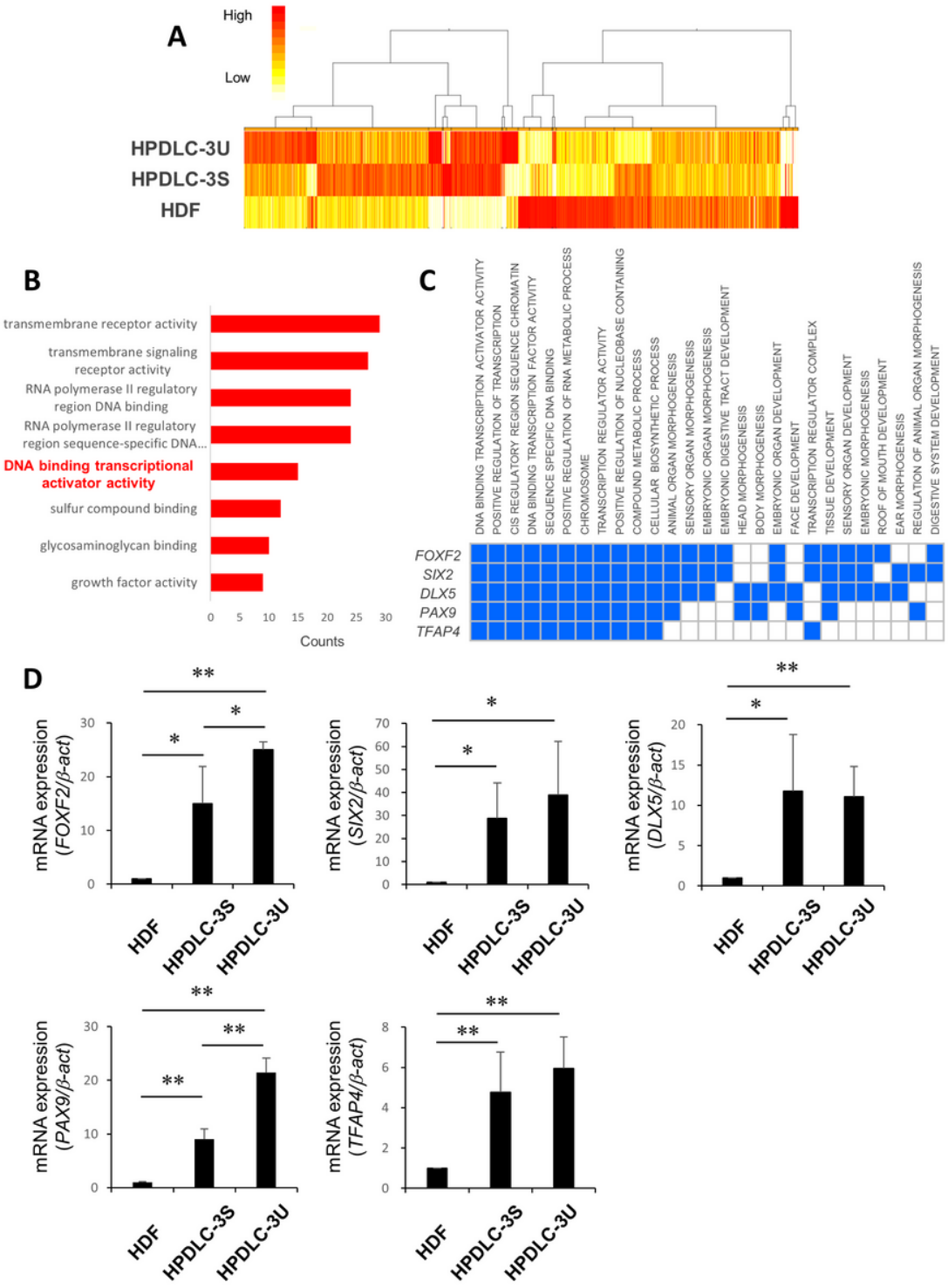

Figure 2

Identification of transcription factor genes highly expressed in HPDLC-3U

A: Heat map and clustering based on hierarchy for gene expression data from CAGE datasets in HDF, HPDLC-3S, and HPDLC-3U. Upregulated genes are represented in red and downregulated genes are represented in yellow. B: GO analysis by BWA software based on upregulated genes in HPDLC-3S compared with HDF in the molecular function group. Data show the top 8 significant terms according to enrichment factor. The term

“DNA binding transcriptional activator activity” included 15 genes. C: GO analysis by GSEA software for *FOXF2*, *SIX2*, *DLX5*, *PAX9*, and *TFAP4*. Blue color means the GO term in which each gene is involved. D: Quantitative real time RT-PCR analysis of *FOXF2*, *SIX2*, *DLX5*, *PAX9*, and *TFAP4* in HDF, HPDLC-3S, and HPDLC-3U. b-act was used as an internal standard. Data are shown as the mean ± standard deviation (n = 4). *P < 0.05, **P < 0.01. CAGE, cap analysis of gene expression; GO, gene ontology; GSEA, gene set enrichment analysis.

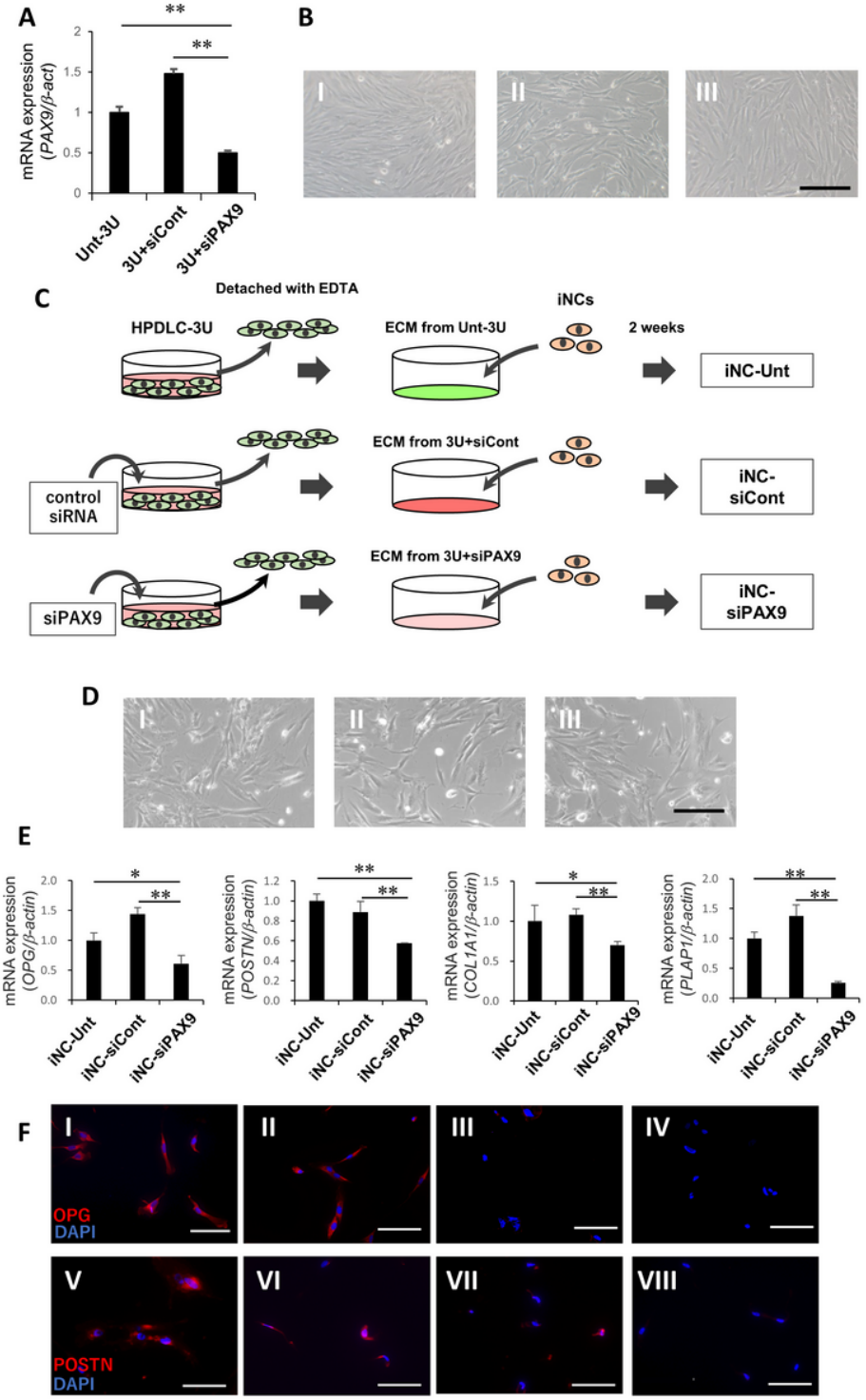

Figure 3

Down-regulation of *PAX9* expression in HPDLC-3U and generation of iNC-Unt, iNC-siCont, and iNC-siPAX9

A: Quantitative real time RT-PCR analysis of *PAX9* in Unt-3U, 3U + siCont, and 3U + siPAX9. b-act was used as an internal standard. Data are shown as the mean ± standard deviation (n = 4). **P < 0.01. B: Representative phase-contrast microscopic images of Unt-3U (I), 3U + siCont (II), and 3U + siPAX9 (III). Bar = 100 mm. Unt-3U, untransfected HPDLC-3U; 3U + siCont, control siRNA-transfected HPDLC-3U; 3U + siPAX9, siPAX9-transfected HPDLC-3U. C: Schema of generation methods for iNC-Unt, iNC-siCont, and iNC-siPAX9. iNCs were cultured for 2 weeks on ECM derived from Unt-3U, 3U + siCont, or 3U + siPAX9B. D: Representative phase-contrast microscopic images of iNC-Unt (I), iNC-siCont (II), and iNC-siPAX9 (III). Bar = 100 mm. E: Quantitative real time RT-PCR analysis of iPDLSC-associated genes *OPG*, *POSTN*, *COL1A1*, and *PLAP1* in iNC-Unt, iNC-siCont, and iNC-siPAX9. b-act was used as an internal standard. Data are shown as the mean ± standard deviation (n = 4). *P < 0.05, **P < 0.01. F: Immunocytochemical staining images of OPG (I-III) and POSTN (V-VII) in iNC-Unt (I, V), iNC-siCont (II, VI), and iNC-siPAX9 (III, VII). iNC-Unt were also stained with control IgG (IV and VIII). The positive reaction was represented by red color. Nuclei were counterstained by DAPI (blue). Bars = 100 mm. iNC-Unt; iNCs cultured on ECM derived from Unt-3U, iNC-siCont; iNCs cultured on ECM derived from 3U + siCont, iNC-siPAX9; iNCs cultured on ECM derived from 3U + siPAX9. ECM, extracellular matrix; iNC, induced pluripotent stem cell-derived neural crest-like cells.

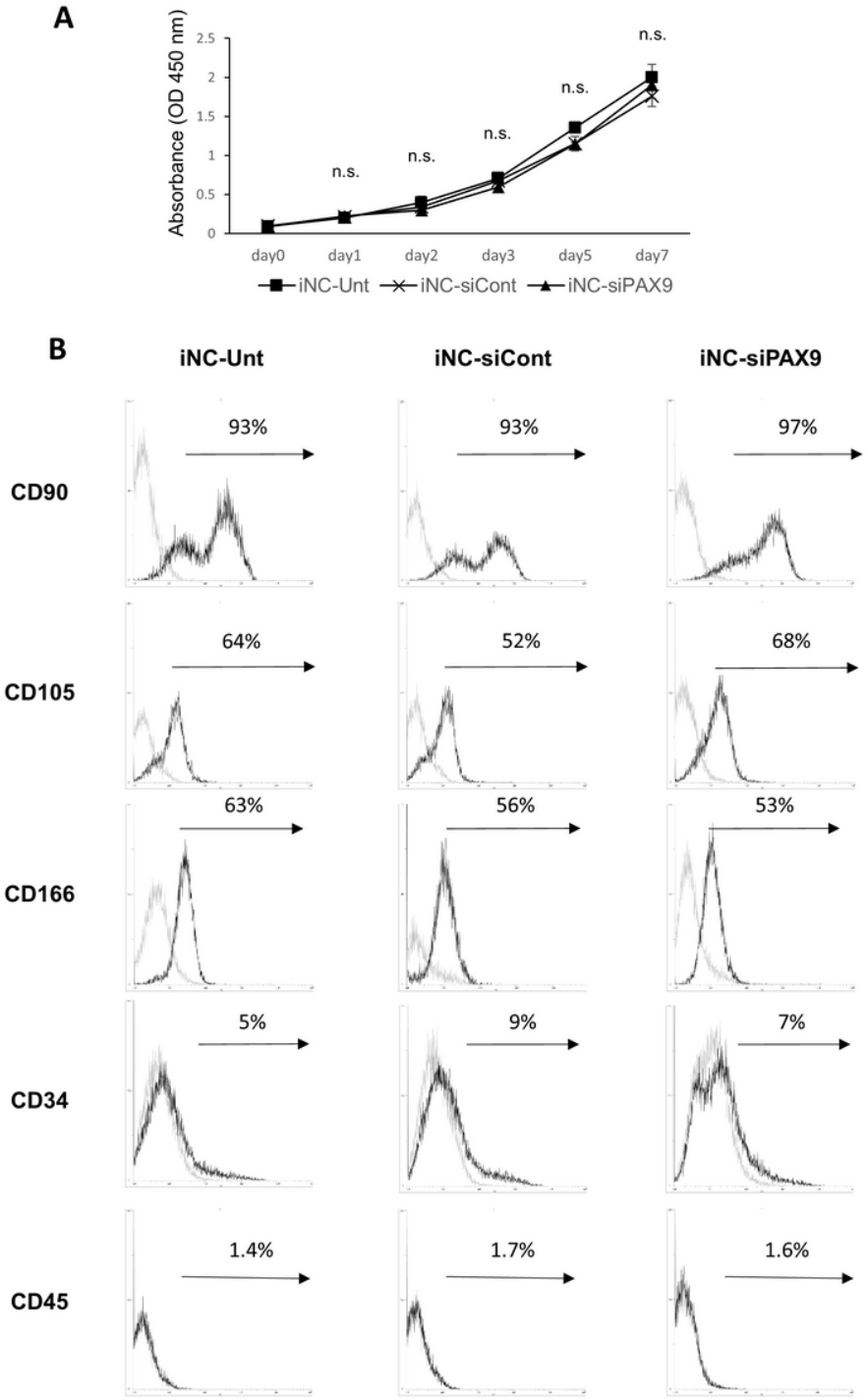

Figure 4

Proliferation and cell surface marker expression in iNC-Unt, iNC-siCont, and iNC-siPAX9

A: Proliferation of iNC-Unt, iNC-siCont, and iNC-siPAX9 determined by WST-1 assay. B: Flow cytometric analysis of MSC (CD90, CD105, and CD166)- and hematopoietic cell (CD34 and CD45)-associated surface marker expression in iNC-Unt, iNC-siCont, and iNC-siPAX9. Histograms showing fluorescently labelled cells

with MSC- and hematopoietic-associated markers (black lines), and isotype-matched control (gray lines). n.s, not significant; iNC, induced pluripotent stem cell-derived neural crest-like cells; MSC, mesenchymal stem cell.

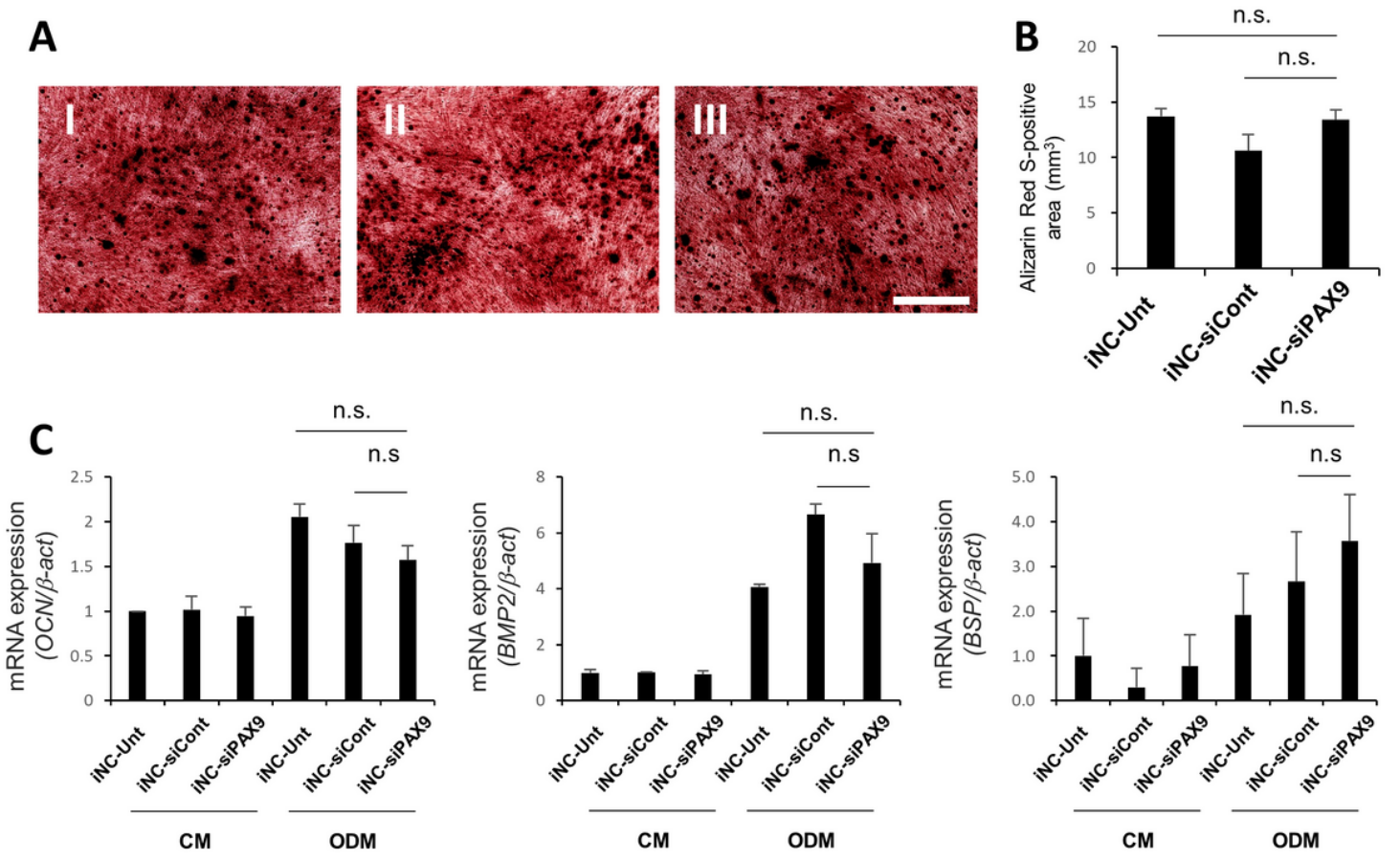

Figure 5

Osteoblastic differentiation of iNC-Unt, iNC-siCont, and iNC-siPAX9

A: Representative Alizarin Red S-staining in iNC-Unt (I), iNC-siCont (II), and iNC-siPAX9 (III) after 3 weeks of culture in ODM. Bar = 100 mm. B: The area of Alizarin Red S-positive staining in iNC-Unt, iNC-siCont, and iNC-siPAX9 cultured in ODM for 3 weeks. C: Quantitative real time RT-PCR analysis of osteoblast-associated marker genes *OCN*, *BMP2*, and *BSP* in iNC-Unt, iNC-siCont, and iNC-siPAX9 after 3 weeks of culture in CM or ODM. b-act was used as an internal standard. Data are shown as the mean ± standard deviation (n = 4). CM; control medium (10% FBS/a-MEM). CM, conditioned medium; iNC, induced pluripotent stem cell-derived neural crest-like cells; ODM, osteoblastic differentiation medium.

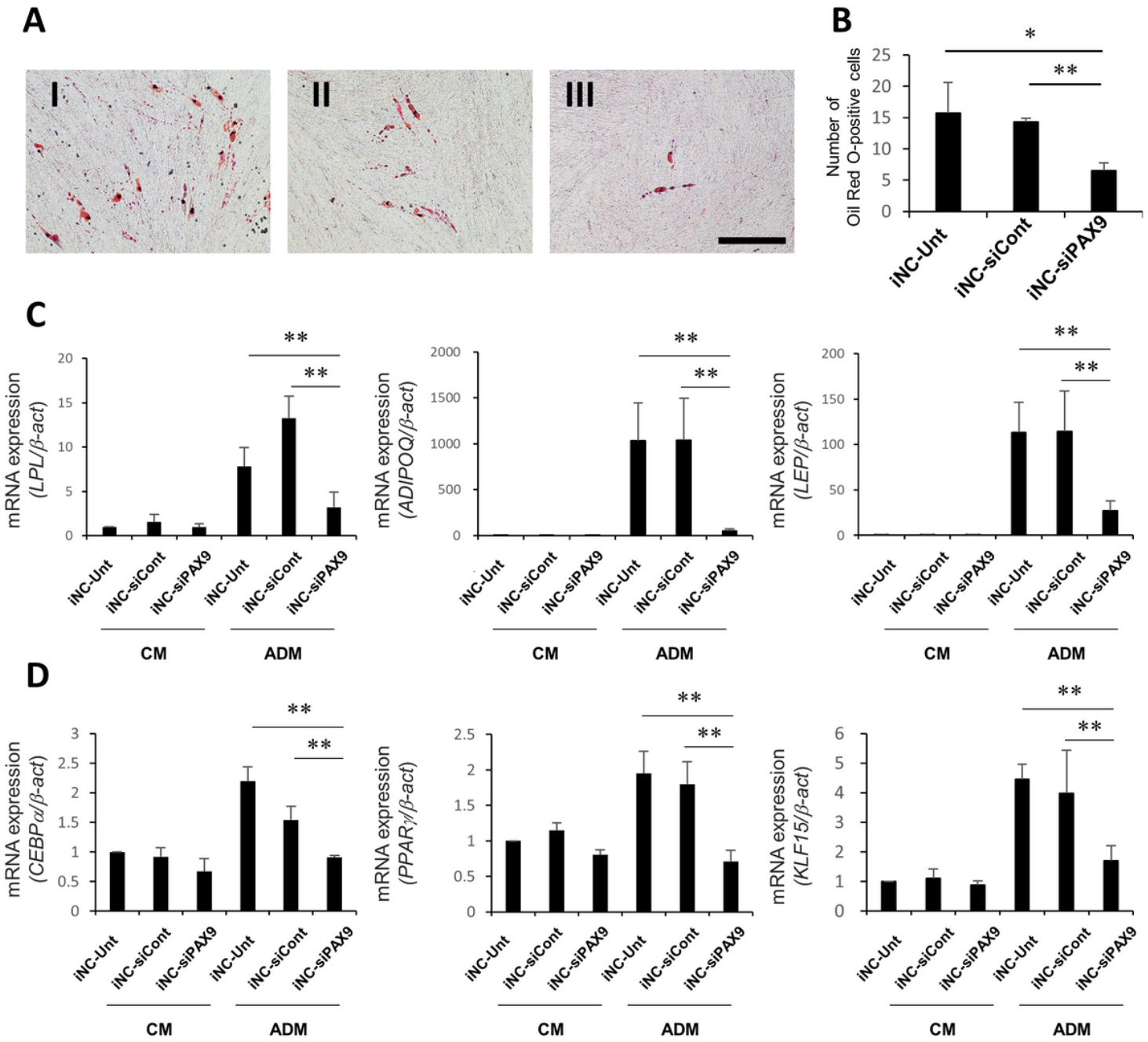

Figure 6

Adipocytic differentiation of iNC-Unt, iNC-siCont, and iNC-siPAX9

A: Representative Oil Red O-staining in iNC-Unt (I), iNC-siCont (II), and iNC-siPAX9 (III) after 4 weeks of culture in ADM. Bar = 100 mm. B: Numbers of Oil Red O-positive cells in iNC-Unt, iNC-siCont, and iNC-siPAX9 cultured in ADM for 4 weeks. C, D: Quantitative real time RT-PCR analysis of adipocyte marker genes *LPL*, *ADIPOQ*, and *LEP*, (C) and adipogenesis regulator genes *CEBPa*, *PPARg*, and *KLF15* (D) in iNC-Unt, iNC-siCont, and iNC-siPAX9 after 4 weeks of culture in CM or ADM. b-act was used as an internal standard. Data are shown as the mean ± standard deviation (n = 4). **P < 0.01. ADM, adipocytic differentiation medium; CM, conditioned medium; iNC, induced pluripotent stem cell-derived neural crest-like cells.

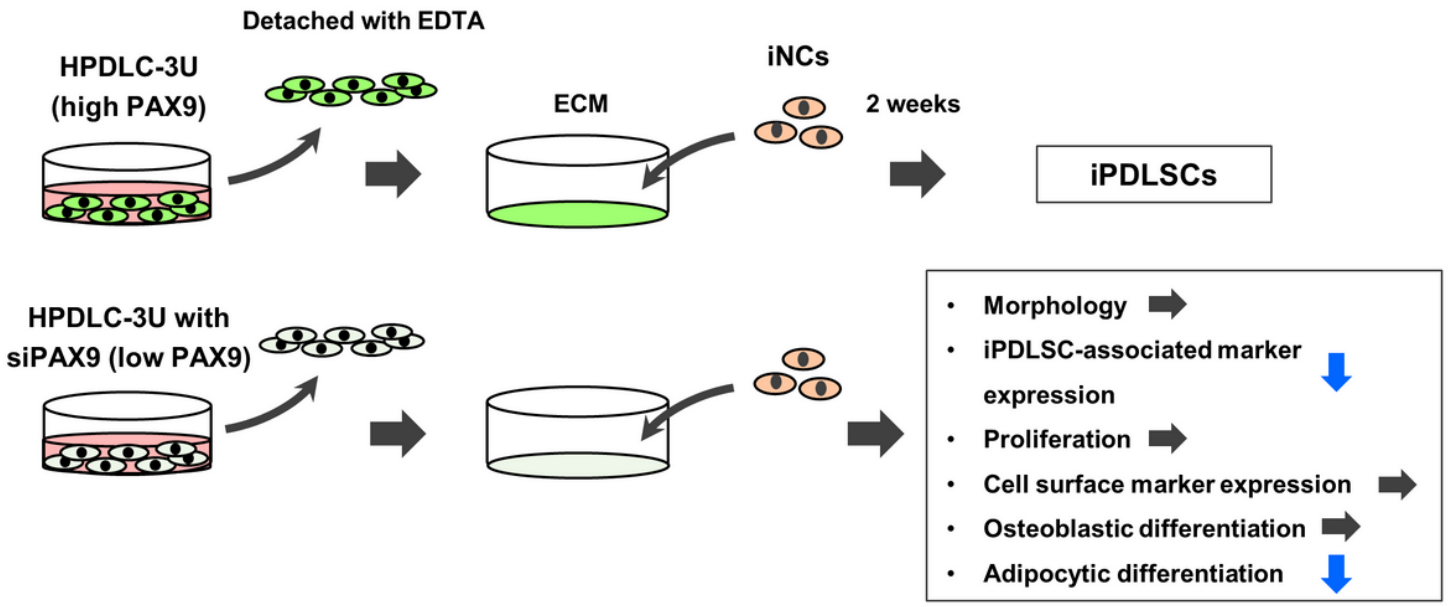

Figure 7

A schematic of the effects of PAX9 downregulation in HPDLC-3U

HPDLC-3U cells highly express *PAX9*, while iNCs cultured on ECM derived from HPDLC-3U differentiate into iPDLSCs. siPAX9-transfected HPDLC-3U downregulates PAX9 gene and protein expression. iNCs cultured on ECM derived from siPAX9-transfected HPDLC-3U decreased the expression of iPDLSC-associated markers and the ability to differentiate into adipocytes. ECM, extracellular matrix; iNC, induced pluripotent stem cell-derived neural crest-like cells.

Supplementary Files

This is a list of supplementary files associated with this preprint. Click to download.

- SupplementFigs.pdf